Fractal Superlattice Cover with Variable Lacunarity For Patch Antenna Directivity Enhancement Analysis and Design

AHMED ALI and HERVE AUBERT

LAAS-CNRS,
7 Avenue du Colonel Roche, 31077,
TOULOUSE, FRANCE.

University of Toulouse
INP-ENSEEIHT
2 rue Charles Camichel, 31071
TOULOUSE, FRANCE.
aali@laas.fr http://www.laas.fr/laas/

Abstract: - The transmission spectrum of fractal polyadic Cantor superlattice exhibits sharp peaks within forbidden frequency gaps. This property has been exploited by placing such self-similar multi-slab structure in the far field radiation region above a radiating element such as a patch antenna to maximize its directivity at the corresponding transmission peak. A patch antenna having directivity of 30 dBi is developed. The design and optimization of the multi-slab structure is achieved using a doubly recursive algorithm. The effect of changing the fractal lacunarity and/or the stage of growth on the transmission characteristics has been studied in both the spectral and spatial domains. Based on accurate analytical expressions for the cover spectral and spatial transmission coefficient, a novel interpretation for the antenna radiation pattern is presented. The antenna including the cover structure is simulated using the moment method-based software tool IE3D. The effect of varying the lacunarity and stage of growth on the spectral and spatial transmission characteristics has been studied analytically using a Matlab program.

Key-Words: - transmission spectrum, self-similar structures, fractal lacunarity, fractal dimension, stage of growth, antenna directivity, Computer-Aided Design (CAD), radiation pattern.

1 Introduction

The spectral transmission characteristics of self-similar stratified media exhibit sharp transmission peaks in high attenuation frequency bands [1]. This property gives rise to many potential applications such as the design of photonic bandgap devices, frequency selective surfaces and selective microwave filters [2-4].

In literature, fractal shapes have been used for different antenna applications, such as antenna miniaturization or multi-band operation. In most of these cases, the fractal shape was applied on the patch level [5].

In this work, self-similar stratified slab structures are used above a patch antenna as a cover to increase its directivity. A simple design procedure is proposed: to have a good physical insight, a simple two-dielectric slabs structure is first studied, then for an improved performance - with more design parameters - another structure is studied by adding more symmetrical dielectric slabs.

Based on a doubly recursive algorithm [6 - 8], the transmission coefficient of the symmetrical multi-slab dielectric cover is calculated for different angles of incidences and their corresponding polarizations. Used as a cover for a patch antenna, the calculated transmission coefficient is then used – for the first time to the authors' knowledge - to explain the radiation pattern of the overall antenna structure. An analogous structure to the studied one has been presented in [9] and experimental results have been reported. However it does not interpret the radiation characteristics nor can it lead to a synthesis procedure as the cover is interpreted as a photonic band gap structure with a defect mode in its transmission bandgaps [10].

Exploring the antenna ground plane and the dielectric cover structure symmetry, half of the cover

structure is used in the electromagnetic simulation to reduce the computation burden [9].

It has been also demonstrated that the separation between slabs is a critical design parameter. Such multi-slab symmetrical structures with variable separations may be regarded as fractal superlattice with variable lacunarity; thus by varying the fractal generator, fractal dimension, stage of growth and especially the fractal lacunarity, the required transmission spectra can be achieved.

2 Cantor Superlattice

In this work, the symmetric multi-slab dielectric structure (Fig.1) - which will be used as a cover for the antenna - is regarded as a fractal Cantor superlattice.
It is generated as a result of an iterative process starting from the initiator (layer of length L and refractive index n_1 corresponding to S = 0 as shown in Fig.1). This layer is immersed in the host medium (air in our case) with refractive index n_o. The cantor superlattice at a certain stage of growth S is obtained by dividing or replacing all layers of stage S-1 into N similar non-overlapping replica scaled by a factor r < 1 while the middle segments generating gaps are replaced by the host medium.

2.1 Fractal Dimension and Lacunarity

In literature, there are many definitions for the fractal dimension [11-14]; in our case, the similarity fractal dimension is adopted as it is the most suitable one for our structure.
The fractal dimension D indicates the amount of space occupied by the fractal structure. The similarity fractal dimension (in the theoretical limit as the stage of growth tends to infinity) is given by [11, 12]

$$D = \frac{\ln N}{\ln r^{-1}} \qquad (1)$$

Therefore, it is clear from both eq. (1) and Fig.1 that, for fixed value of N, cantor bars with larger amount of mass removed have lower fractal dimension. It is also clear that we may have different sets of fractal Cantor bars having the same fractal dimension with different gap sizes and therefore different shapes.

This highlights the fact that the fractal dimension is not sufficient to describe the fractal structure. Another crucial fractal descriptor is defined to provide additional information about fractal structures which is the fractal lacunarity.

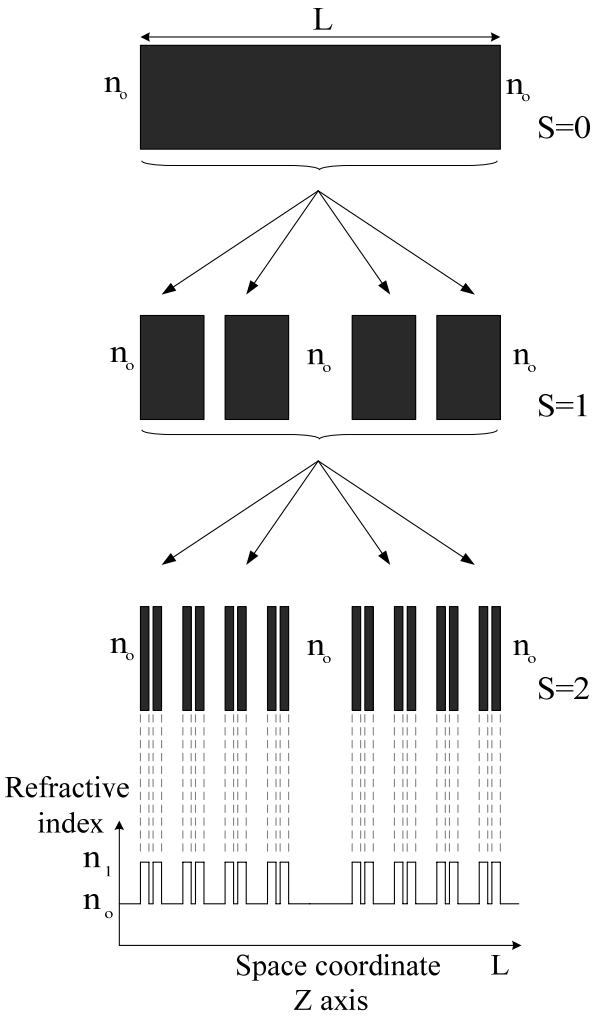

Fig.1 Schematic of the iterative process illustrating the construction of a Cantor superlattice with variable lacunarity from S = 0 to S = 2.

The term lacunarity was introduced by Mandelbrot [15] to describe the degree of homogeneity of a fractal. In our case of interest for the symmetric Cantor sets, lacunarity is characterized by the normalized width of the outermost gap in the first stage of growth (S=1), therefore, the more the structure is translationally variant and inhomogeneous, the more it is lacunar and vice versa. Numerous definitions can be found in literature to define this fractal descriptor [15-17].

3 Problem Statement and Analysis

In this section, the transmission coefficient of the cover structure is calculated analytically for different angles of incidences and their corresponding polarizations for plane wave incidence. This calculated transmission coefficient is used to explain the radiation pattern of the antenna and the relative directivities of antennas using different cover structures.
Exploring the symmetrical characteristics and the recursive iterations of the cover structure, a doubly

recursive algorithm [6-8] is used to provide accurate and fast analytical expressions for the transmission coefficient for plane wave incidence on the cover.

The doubly recursive algorithm consists of a pair of recursions analogous to the iterative constructive process for the cover: the first recursion is accomplished on the level of the number of gaps or in other words accounts for the reflection and transmission at the individual interfaces. This recursion ends up by constructing the generalized reflection and transmission functions $g_r(x,y,L)$ and $g_t(x,y,L)$ as follows:

$$g_r(x,y,L) = gen_r(n_{gaps}) \tag{2}$$

$$g_t(x,y,L) = gen_t(n_{gaps}) \tag{3}$$

$$gen_r(n_{gaps}) = \frac{x + (y^2 - x^2)\, gen_r(n_{gaps}-1)\exp(2\,i\,n_o k\,\alpha_i L\cos\theta_o)}{1 - x\, gen_r(n_{gaps}-1)\exp(2\,i\,n_o\, k\,\alpha_i L\cos\theta_o)} \tag{4}$$

$$gen_t(n_{gaps}) = \frac{y\, gen_t(n_{gaps}-1)\exp(2\,i\,n_o\, k\,\alpha_i L\cos\theta_o)}{1 - x\, gen_r(n_{gaps}-1)\exp(2\,i\,n_o\, k\,\alpha_i L\cos\theta_o)} \tag{5}$$

With the initial conditions

$$gen_r(0) = x \qquad gen_t(0) = y \tag{6}$$

Where n_{gaps} denotes the number of gaps such that $n_{gaps} \geq 1$, k is the free space-space wave number of the incident wave, α_i (i= 1,2,..,n_{gaps}) denotes the gap sizes normalized to the total length L, and θ_o is the angle of incidence as shown in Fig. 2.

The second recursion is on the stage of growth level where the transmission coefficient at a certain stage of growth S with a corresponding length L_S is calculated by replacing the generalized transmission coefficient above by the transmission (reflection) coefficient of a Cantor bar at stage of growth S-1 with a length of RL_{S-1} as described by eq.7 and 8.

$$R(S,L) = g_r\left[R(S\text{-}1),\, rL_{S-1},\, T(S\text{-}1,\, rL_{S-1}),L\right] \tag{7}$$

$$T(S,L) = g_t\left[R(S\text{-}1),\, rL_{S-1},\, T(S\text{-}1,\, rL_{S-1}),L\right] \tag{8}$$

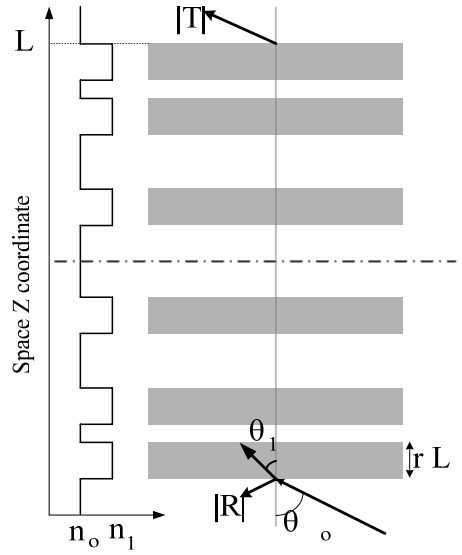

Fig. 2 Five-gap Cantor superlattice with variable lacunarity at the first stage of growth with plane electromagnetic wave with oblique incidence, |R| represents the magnitude of the wave reflection coefficient while |T| represents that of the transmission coefficient.

The initial conditions for these relations are given by the well-known reflection and transmission coefficients for a slab of a certain length d – corresponding to r^S L- with refractive index n_1 embedded in an infinite region of refractive index n_o as;

$$R(0,d) = \frac{r_{01} + (t_{10}\, t_{01} - r_{01}\, r_{10})\, r_{10}\exp(2\,i\,n_1 k\,d\cos\theta_1)}{[1 - r_{10}{}^2\exp(2\,i\,n_1\, k\,d\cos\theta_1)]} \tag{9}$$

$$T(0,d) = \frac{t_{01}\, t_{10}\exp(i\,n_1\, k\,d\cos\theta_1)}{[1 - r_{10}{}^2\exp(2\,i\,n_1\, k\,d\cos\theta_1)]} \tag{10}$$

Where

$$r_{ij} = -\frac{\hat{n}_i - \hat{n}_j}{\hat{n}_i + \hat{n}_j} \tag{11}$$

$$t_{ij} = -\frac{2\hat{n}_i}{\hat{n}_i + \hat{n}_j}\vartheta_{ij} \tag{12}$$

are the Fresnel reflection and transmission coefficients respectively, for an interface between two media of refractive indices n_i and n_j with:

$$\vartheta_{ij} = \begin{cases} \cos\theta_i / \cos\theta_j & \text{for parallel polarization} \\ 1 & \text{for perpendicular polarization} \end{cases} \tag{13}$$

$$\hat{n}_i = \begin{cases} n_i / \cos\theta_i & \text{for parallel polarization} \\ -n_i \cos\theta_i & \text{for perpendicular polarization} \end{cases} \quad (14)$$

Relations (2)-(14) allow obtaining accurate expressions for the transmission coefficient across the cover structure for any angle of incidence, polarization and gap distributions (lacunarity) which will be used in the following sections.

4 Spectral and Spatial Transmission Characteristics of Symmetrical Multi-Slab Dielectric Structures:

For good understanding of the multi-slab performance, a simple structure of two-dielectric slabs (denoted by cover (1)), as shown in Fig. 3(a), is investigated first. As the structure is symmetrical, the design parameters are simply the air gap width h_1,

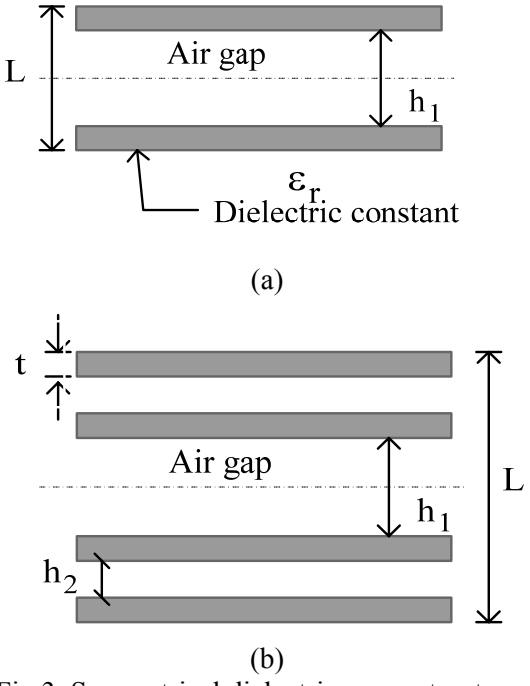

Fig.3. Symmetrical dielectric cover structures: (a) Two-dielectric slabs *(cover 1)*. (b) Four-dielectric slabs structure *(cover 2)*.

the dielectric constant ε_r and the dielectric thickness t (t = rL). These design parameters are chosen to obtain a bandgap in the transmission spectrum with a transmission peak. This transmission peak must coincide with the resonant frequency of the patch antenna beneath the cover.

Since the transmission peaks represent the resonances of the individual layers (cavities) and/or those of groups of layers, for simple structures as that of Fig. 3 (a), the middle air gap width can be chosen approximately equal to integer multiple of half the wavelength corresponding to the antenna operating frequency.

The transmission spectrum for a plane wave at normal incidence on the structure of Fig.3 (a) is shown in Fig. 4 (a). The structure has been designed to obtain a transmission peak at 2.4 GHz. The design parameters are as follows: h_1=123.14 mm, t = 7.14 mm and the dielectric used is the (Sm $(Co_{1/2},Ti_{1/2})O_3$ dielectric with ε_r = 25.5.

Although the design procedure of this structure can be easily optimized, this structure is not practical as once the air gap thickness is determined, the only design parameters that can be controlled are the dielectric parameters that are normally governed by the available dielectric laminates with their commercial discrete thicknesses. Therefore, at least one more design parameter is required. This is accomplished by adding one (or more) couple(s) of symmetrical dielectric slabs to the previous structure leading to the structure of Fig. 3(b) denoted by cover (2).

Comparing both structures of Fig. 3 (a) and (b), it is clear that the structure of Fig. 3(b) has one more design parameter over that of (a) which is h_2, considering that all dielectric slabs are identical.

Fig. 4 (b) shows the transmission spectrum of the designed cover structure of Fig. 3 (b) for a plane wave at normal incidence. The designed structure has the same design parameters of Fig.3 (a) previously discussed, while the new design parameter; h_2 has been varied from 8 mm to 16 mm.

By comparing Fig. 4 (a) and (b), the critical effect of "h_2" is clarified as it can be adjusted to fine tune the transmission peak to the required frequency value. Furthermore, it can be noted that the addition of new dielectric layers (Fig. 3 (b) and Fig.4 (b)) can be used to control the transmission bandgaps depths leading to more selective cover structures.

Therefore, for specified dielectric slab cover structure; by adjusting the central air-gap size and choosing an appropriate value for h_2, the transmission peak can be adjusted to the required frequency.

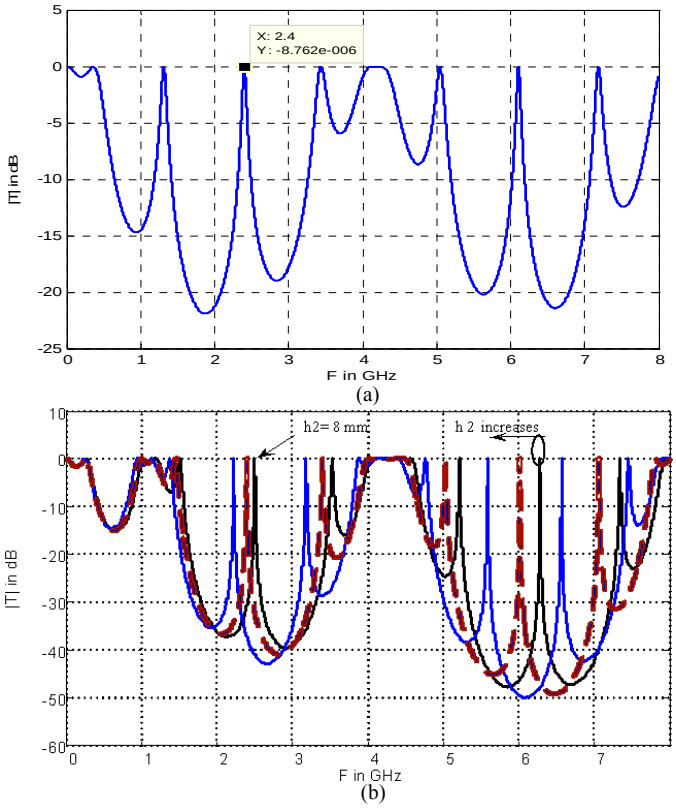

Fig. 4. Transmission coefficient in dB against frequency for a plane wave at normal incidence:
(a) Two-dielectric slab structure, $h_1 = 123.14$mm, $\varepsilon_r = 25.5$, $t = 7.14$ mm. (b) Four-dielectric slabs structure for different values of $h_2 = 8$, 12.1 and 16 mm, other parameters are same as (a).

Moreover the transmission coefficient of both covers (1) and (2) has been calculated for different angles of incidences and their corresponding polarizations while ensuring a transmission peak for both structures at normal incidence at the same frequency (2.4 GHz in our case). By comparing the calculated results shown in Fig. 5, we note that the 3-dB beam width has been significantly narrowed from 20^o (cover (1)) to about 6^o (cover (2)). This narrow beam-width is consequently expected to achieve an increased directivity if the dielectric structure is illuminated by a broadside antenna which will be verified in the next section.

4.1 Effect of stage of growth

In this section, the effect of the stage of growth is studied for both spectral and spatial transmission characteristics. Fig. 6 shows the spectral transmission coefficient versus frequency for the cover structure of Fig. 3(b) at the second stage of growth. While the spatial transmission characteristics are shown in Fig. 7 for both parallel and perpendicular polarizations for the first transmission maximum at 9 GHz.

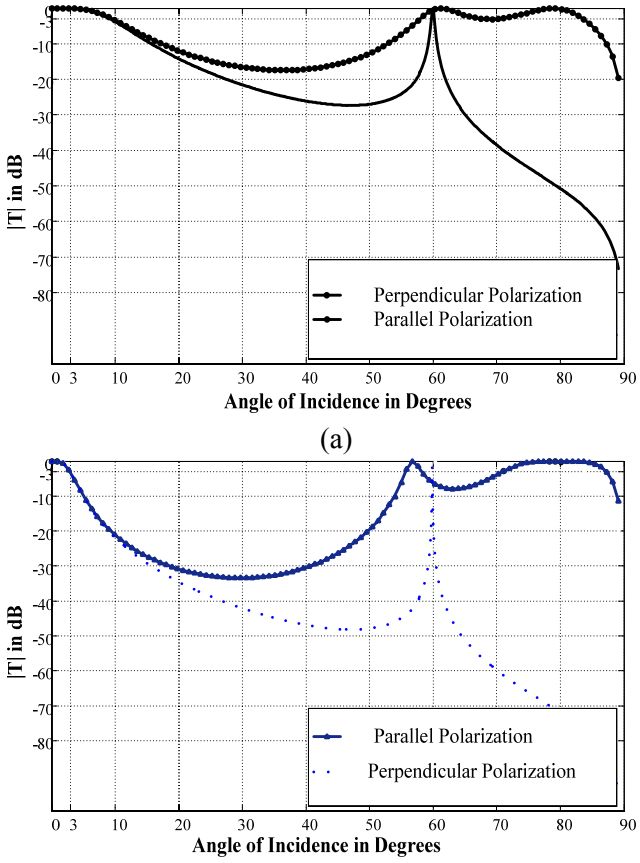

Fig. 5 Calculated spatial transmission coefficient of at 2.4 GHz for parallel and perpendicular polarizations for different angles of incidence: (a) Cover 1, (b) Cover 2.

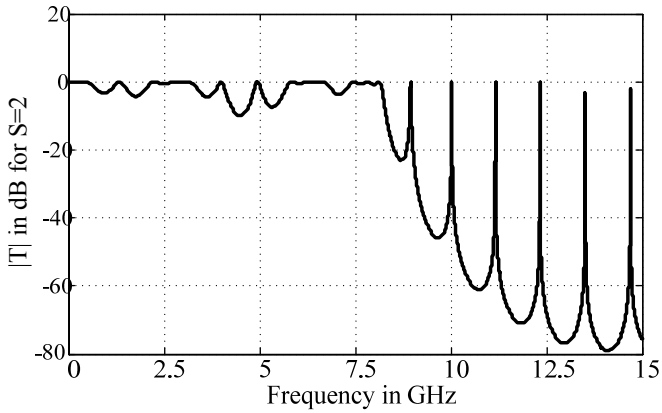

Fig. 6 Transmission coefficient in dB versus frequency for plane wave incidence on cover 2 with $h_1 = 123.14$mm, $\varepsilon_r = 25.5$, $t = 7.14$ mm ($r = t/L = 0.0426$), $h_2 = 8$mm at the second stage of growth (S=2)

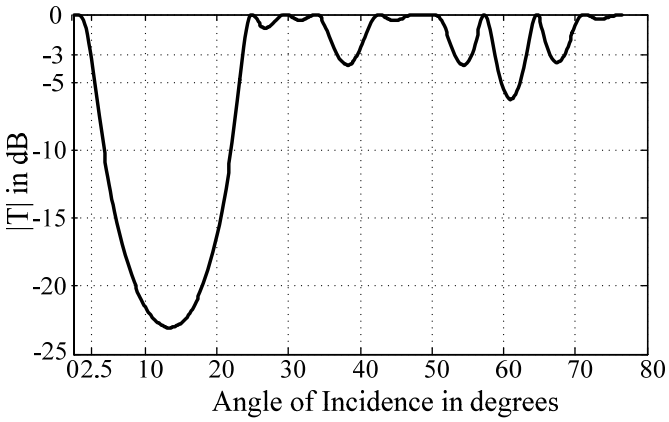

(a)

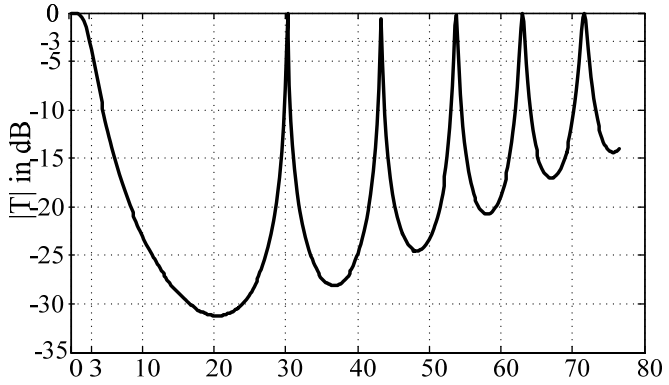

(b)

Fig. 7 Calculated spatial transmission coefficient of at the first transmission peak of Fig.6 (9.0 GHz): (a) parallel polarization, (b) perpendicular polarization

By comparing the transmission characteristics of cover 2 for the S=1 case (the curve corresponding to h_2 of 8 mm in Fig.4 (b) and Fig. 5 (b) for spectral and spatial characteristics respectively), and S = 2 (Fig.6 and Fig.7), we can conclude the following remarks:

- By increasing the stage of growth for the same lacunarity and fractal dimension, the transmission bandgaps become deeper with sharper (more selective) transmission maxima;
- The transmission maxima are shifted to higher frequencies which is a natural effect since they correspond to the resonances of the different cavities, the amount of shift depends on the iteration number (stage of growth) and the refractive index n_1.
- For higher stages of growth, the spatial transmission coefficient maxima become closer to the broadside direction than for the case of S=1, this property shall invoke higher side lobe levels (for the case S>1) if these covers are illuminated by patch antennas especially for the parallel polarization field component (as the perpendicular polarization component has relatively narrower transmission maxima with respect to the maximum at broadside direction, $\theta = 0$).

4.2 Effect of Lacunarity

In this section, the effect of lacunarity on the transmission characteristics is investigated. The lacunarity of the cover structure of Fig.3 (b) has been change from the previously studied values of Fig.4 (b) and Fig.5 (b) [h_1 = 123.14mm, h_2 = 8mm] to [h_1 = 103.14mm, h_2 = 18mm] while maintaining all the other fractal parameters, and therefore the lacunarity has been lowered.

Fig. 8 shows the calculated transmission spectrum with the new lacunarity for both S = 1 and S = 2, while Fig.9 shows the calculated transmission coefficient versus the incidence angle for the corresponding frequency of the first transmission maximum for both values of S. By comparing the results of Fig. 8 and Fig. 9 with those of Fig. 4(b)-Fig.7 we can see the critical effect of the lacunarity on shifting the positions of the transmission maxima. This shift is very useful in the design of such covers for highly directive patch antennas as it can be controlled by choosing the appropriate values for the gap sizes.

Although the fractal stage of growth has an effect on the transmission maxima positions, the effect of changing the lacunarity is more useful since the shift is slow and we can keep reasonable values of the dielectric layers thicknesses which is not the case for the corresponding theoretical thin thicknesses in the case of higher iterations.

On the other hand, the same conclusions for the stage of growth effects mentioned in the previous section are verified.

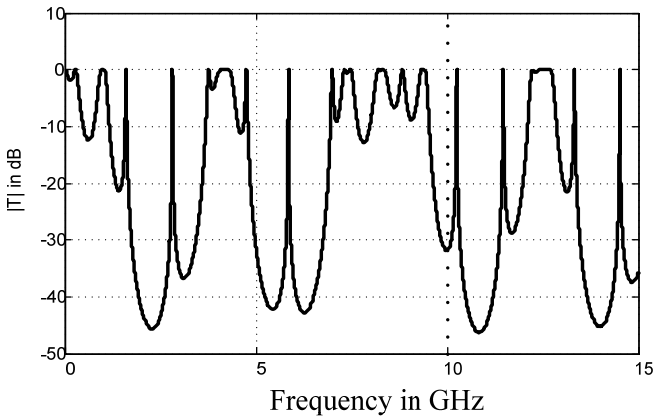

(a)

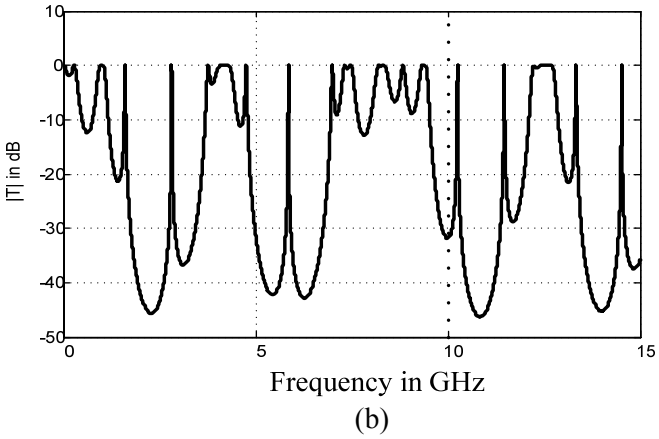

(b)

Fig. 8 Transmission coefficient in dB versus frequency for plane wave incidence on the structure of Fig.3 (b) with h_1 = 103.14mm, ε_r = 25.5, t = 7.14 mm (r = t/L = 0.0426), h_2=18mm, (a)S = 1, (b) S = 2

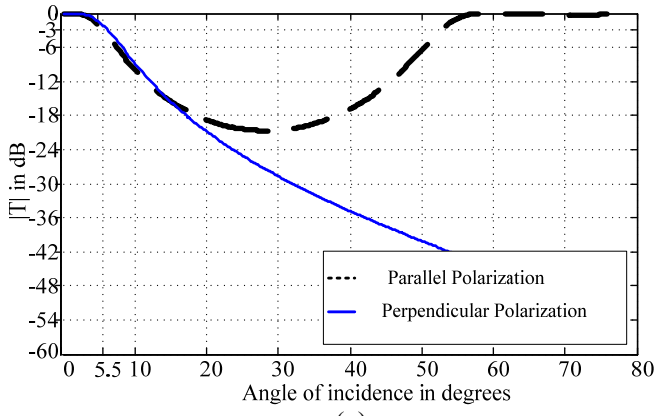

(a)

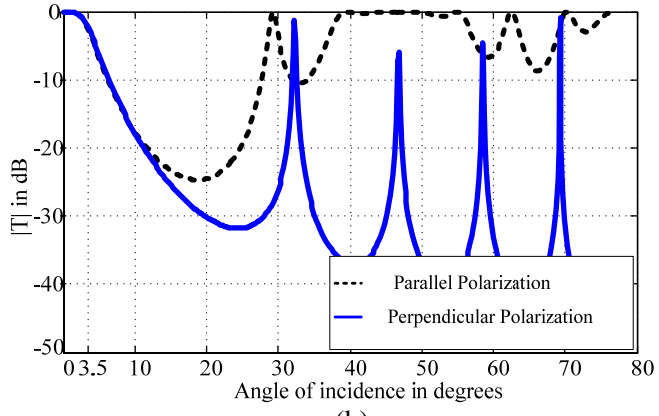

(b)

Fig. 9 Calculated spatial transmission coefficient for parallel and perpendicular polarizations for different angles of incidence for the structures of Fig.8, (a) the first transmission maximum of Fig. 8 (a) at F = 1.6 GHz (b) the first transmission maximum of Fig. 8 (b) at F = 9 GHz.

5 Design and Results:

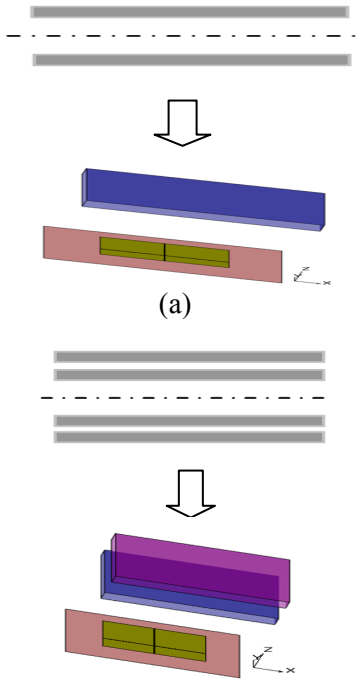

(a) (b)

Fig.10. The overall physical structure of the simulated antennas: (a) Antenna (1), (b) Antenna (2).

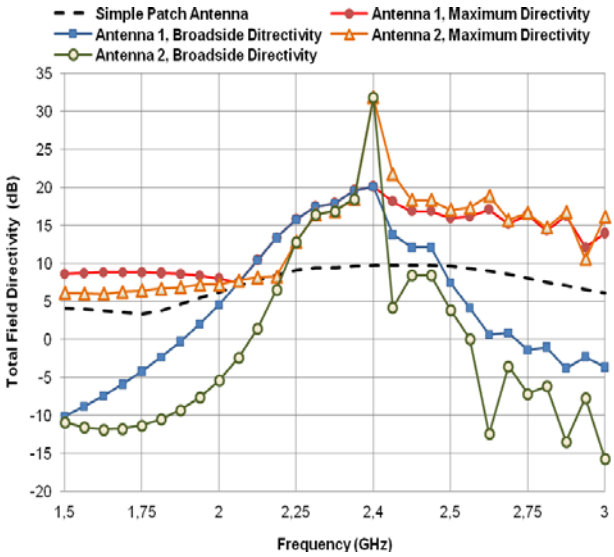

Fig. 11 Simulated total field maximum and broadside directivities for antennas (1) and (2) compared to that of the simple patch antenna without cover.

In this section, the previously designed symmetrical multi-slab dielectric structures are applied as a cover for a patch antenna. The structural parameters of the covers are those of Fig.4 with h_2 = 8 mm for cover (2). A computer-aided design (CAD) is carried out by an optimization program applying the calculated transmission coefficient for the cover. This optimization

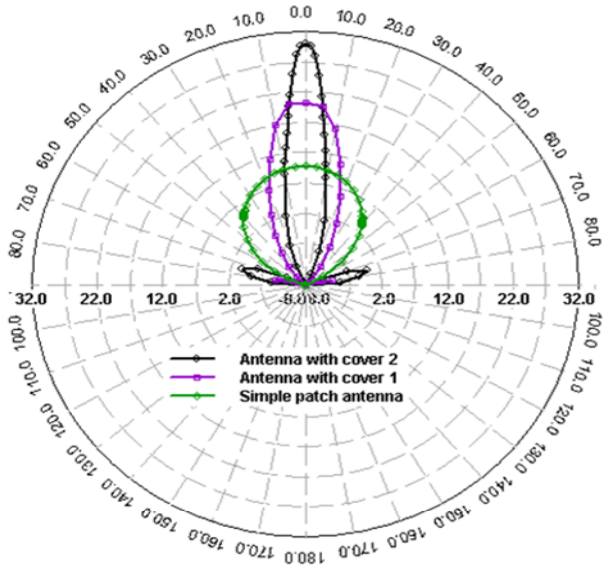

(a)

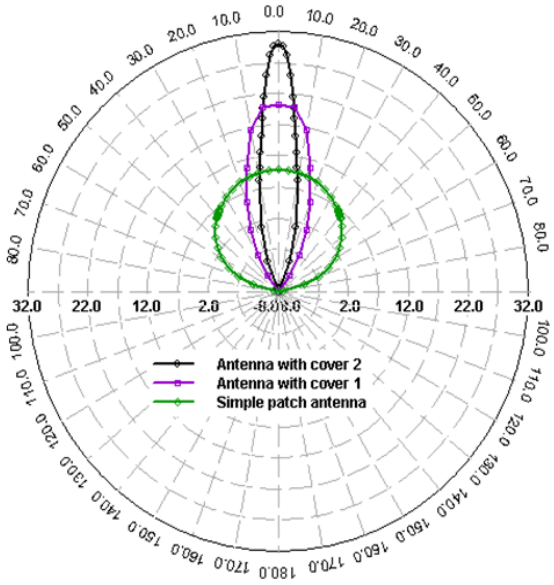

(b)

Fig. 12. (a) Simulated E_θ radiation pattern of the designed antenna with and without covers in the $\varphi=90^o$ plane: parallel polarization. (b) Simulated E_φ elevation radiation pattern for the $\varphi=0$ plane: perpendicular polarization, at F = 2.4 GHz

program varies the cover parameters (ε_r, t, h and the air-gap width(s)) until the desired transmission characteristics for a given bandwidth and direction are obtained. To maintain validity of the analytical equations discussed in section 3, plane wave incidence must be insured. Therefore, the covers must be placed in the far field radiation region of the illuminating antenna. The antenna, including the optimized cover structure, is then simulated using the full-wave, MoM based IE3D simulator [18].

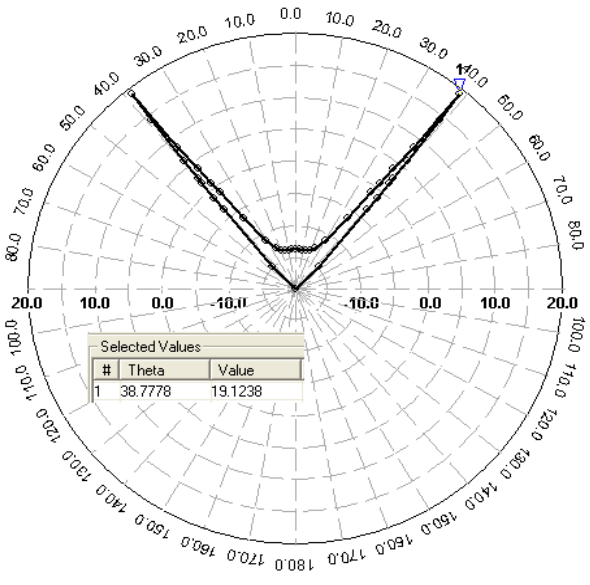

(a)

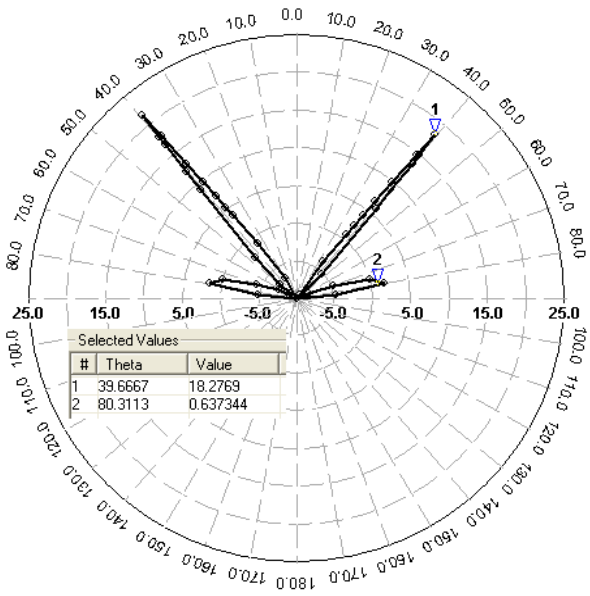

(b)

Fig. 13. (a) Simulated E_θ radiation pattern of the designed antenna with cover 2 in the $\varphi=90^o$ plane: parallel polarization. (b) Simulated E_φ elevation radiation pattern for the $\varphi=0$ plane: perpendicular polarization, at F = 2.6 GHz

Experimental validation results for similar structures have been previously reported [9]. Both of the previously discussed cover structures have been used in the simulation. The dielectric loss (tan δ = 0.00013) and the conductor losses have been taken into account in the simulation. The whole simulated antenna structure is composed of the patch antenna and the upper half of the cover structure (placed at a distance $h_1/2$), as presented in Fig. 10, the antenna applying cover (1) is referred to by antenna (1) and that applying cover (2) is referred to

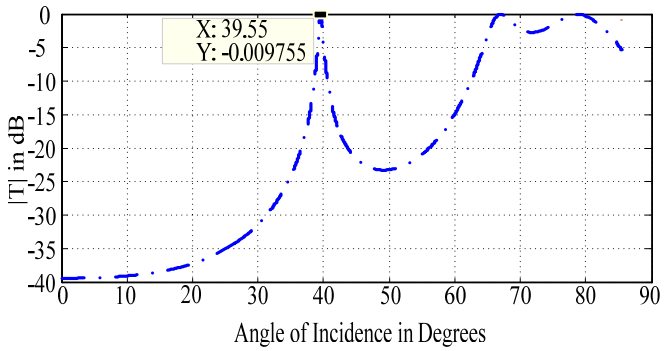

(a)

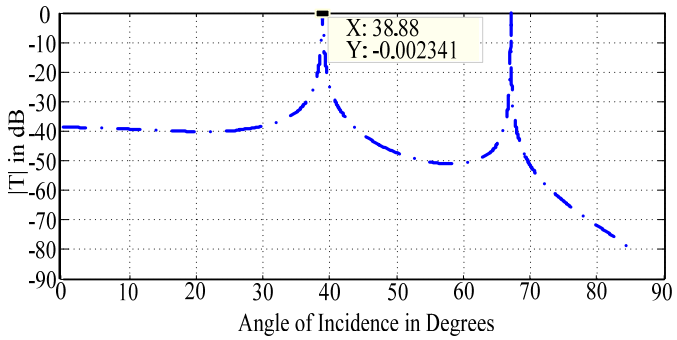

(b)

Fig. 14 Calculated spatial transmission coefficient for parallel and perpendicular polarizations for different angles of incidence for cover (2) at 2.6 GHz, (a) parallel polarization, (b) perpendicular polarization.

by antenna (2).Both antennas are probe-fed and have a 2.7 mm thick air substrate and designed to operate at 2.4 GHz.

Fig. 11 shows the simulated total field directivity versus frequency in the broadside direction as well as the maximum total field directivity for both antennas (1) and (2) in addition to the simple un-covered patch antenna. For the antenna (1), there is a great agreement between the electromagnetic simulation results and the calculated transmission coefficient of cover (1), as the maximum broadside directivity is at 2.4 GHz. It can be seen that the antenna total broadside directivity has been doubled at the desired design frequency.

The same agreement applies for the simulated results for the antenna (2) and the calculated transmission characteristics of the corresponding cover.

From Fig. 11, for antenna (2) it can be seen that the antenna total broadside directivity has been doubled over the frequency range from 2.3 GHz to 2.45 GHz achieving a 6.25% broadside directivity bandwidth defined by 20 dBi with its maximum at 2.4 GHz, where the directivity value has been almost tripled (about 31 dBi) compared to that of the simple un-covered probe-fed patch antenna (9.7dBi).

Fig.12 (a) and (b) show the radiation patterns of both antennas (1) and (2), compared to the reference uncovered one in both E and H planes at 2.4 GHz. The simulated covered antenna radiation efficiency is almost 100 % at 2.4 GHz. By comparing Fig. 5 with the radiation patterns of Fig.12, great agreement between the calculated transmission characteristics and the simulated radiation patterns is clearly verified. The simulated 3-dB beamwidths for both antennas (1) and (2) agrees with the previously discussed calculated ones of the corresponding covers in Fig.5 which explains the increased directivity of antenna (2) compared to antenna (1).

Fig. 13 shows the radiation patterns of antenna (2) for a case where the maximum directivity is not at broadside at 2.6 GHz. By comparing Fig. 13 with the calculated transmission characteristics of Fig.14 for parallel and perpendicular polarizations, the same agreement is clearly verified.

This agreement between calculated and simulated results allows us to interpret the spatial power distribution within the radiation pattern for the multi-slab dielectric covered antenna structures. The power radiation is normally forbidden in the spatial transmission gaps and then is re-distributed according to the directions of the transmission maxima and their relative bandwidths to each other; this latter parameter governs the relative directivities at each radiation lobe at the corresponding transmission maximum for the same frequency.

In other words, the new radiation pattern of the covered antenna is mapped to its spatial transmission maxima and has relative directivities related to the relative bandwidths of these maxima. Consequently, for a given frequency, if the spatial transmission coefficient has a very narrow transmission peak as compared to the other one, no radiation in the direction corresponding to that peak will occur.

6 Conclusion

The direct correlation between the radiation pattern of dielectric, symmetrical superlattice covered patch antennas and the calculated spectral and spatial transmission spectra for the superlattice cover structure allows an optimized, accurate, computer-based synthesis for highly directive patch antennas. The cover structure is first studied analytically and optimized using CAD program then the whole antenna structure is simulated for validation.

References:

[1] D. Jaggard, L. Jaggard, Reflection from fractal mulilayers, *Optical Letters*, Vol. 15, No. 24, 1990, pp. 1428-1430.

[2] A. S. Saleh, and H. Aubert, Use of variable lacunarity, multi-gap, Cantor slabs in waveguides

for the design of microwave filters, *Microwave Optical and Technological Letters*, Vol. 28, Issue 2, 2001, pp.127-130.

[3] A. S. Saleh, and H. Aubert, Self-similar multi-slab media with variable lacunarity for design of selective microwave filters, *Electronic Letters*, Vol. 37, No. 17, August 2001, pp. 1071-1073.

[4] F. Surre, A. S. Saleh and H. Aubert, Frequency response of self-similar planar waveguides, *Microwave Optical and Technological Letters*, Vol. 37, Issue 3, 2003, pp.208-210.

[5] M. Ismail, H. Elsadek, E. A. Abdallah and A. A. Ammar, Modified pulse 2.45 Fractal microstrip antenna, *WSEAS transactions on communications*, Vol. 7, Issue 4, April 2008, pp. 280-288

[6] D. L. Jaggard and X. Sun, "Reflection from Fractal Layers," *Optical Letters* Vol.15, No. 24, 1990, pp. 1428-1430.

[7] X. Sun and D. L. Jaggard, "Wave Interactions with generalized Cantor Bar Fractal Multilayers," *Journal of Applied Physics*, Vol. 70, 1991, pp. 2500-2507.

[8] D. Jaggard, L. Jaggard, Scattering from fractal superlattice with variable lacunarity, *Journal of Optical Society of America A*, Vol. 15, No. 6, June 1998, pp. 1626-1635.

[9] M. Thèvenot, C. Cheype, A. Reineix and B. Jecko, Directive Photonic-Bandgap Antennas, *IEEE Transactions on Microwave Theory and Techniques*, Vol. 47, No. 11, Nov. 1999, pp. 2115-2122 .

[10] G. S. Kliros, K. S. Liantzas, and A. A. Konstantinidis, Radiation Pattern Improvement of a Microstrip Patch Antenna using Electromagnetic Bandgap Substrate and Superstrate, *WSEAS Transactions on Communications,* Vol.6, Jan. 2007, pp. 45-52.

[11] Stanley H. E. and N. Ostrowsky, eds., *On Growth and Form: Fractal and Non-Fractal Patterns in Physics,* Nijhoff, Boston, 1986.

[12] B. B. Mandelbrot, *The Fractal Geometry of Nature,* Freeman, New York, 1983.

[13] K. Harrar, L. Hamami, The box counting method for evaluating the fractal dimension in radiographic images, *6th WSEAS international conference on circuits, systems, electronics, control & signal processing,* 2007, pp. 385-390.

[14] K. Harrar and L. Hamami, The fractal dimension correlated to the bone mineral density, *WSEAS transactions on signal processing,* Vol.4, Issue 3, March 2008, pp. 110-126.

[15] B. B. Mandelbrot, ''A fractal's lacunarity, and how it can be tuned and measured,'' *Fractals in Biology and Medicine*, T. F. Nonnenmacher, G. A. Losa, and E. R. Weibel, 1994.

[16] D. A. Fa´ bio, A. Reis, and R. Riera, Lacunarity calculation in the true fractal limit, *Journal of Physics A,* Vol. **27**, 1994, pp. 1827-1835.

[17] C. Allain and M. Cloitre, Characterizing the lacunarity of random and deterministic fractal sets, *Phys. Rev. A* ,Vol.44, 1991, pp.3552–3558 .

[18] IE3D Version 12.1, Zeland Software Inc., June 2007.